THE JOURNAL OF PHYSICAL CHEMISTRY C
A JOURNAL OF THE AMERICAN CHEMICAL SOCIETY

pubs.acs.org/JPCC

Article

Differentiating Intra-Assembly and Interlayer Energy Transfer in Metal-Ion-Linked Molecular Multilayers

Grace M. McLeod, Jackson Nolder, Ashley Arcidiacono, Sarah Lindbom, Nikolas R. Dos Santos, Ethan C. Lambert, Suliman Ayad, Drake Beery, Igor V. Alabugin, and Kenneth Hanson*

Cite This: J. Phys. Chem. C 2024, 128, 16861−16868

Read Online

ACCESS | Metrics & More | Article Recommendations | Supporting Information

ABSTRACT: Metal-ion-linked molecular multilayers on metal oxide surfaces are promising for applications ranging from solar energy conversion to sensing. Most of these applications rely on energy and electron transfer between layers/molecules which can be envisioned to occur via intra-assembly (IA; between metal-ion-linked molecules) and interlayer (IL; between separate layers of nonlinked molecules) processes. Here, we describe our effort to differentiate between IL and IA energy transfer using a bilayer composed of ZrO_2, a phosphonated anthracene derivative (A), a zinc(II) linking ion, and a Pt(II)porphyrin (P). Both time-resolved emission and transient absorption measurements show no impact of diluting the anthracene layer with a spectroscopically inert spacer on the rate of ^{1}A* to P and ^{3}P* to A, singlet, and triplet energy transfer, respectively. These results indicate that energy transfer within the metal-ion-linked assembly (i.e., ZrO_2-**A**−Zn-**P**) is more rapid than with an adjacent, nonlinked A molecule, even for a P derivative capable of laying down on the surface. These insights are an important step toward structural design principles maximizing the efficiency/rate of energy transfer in multilayer assemblies.

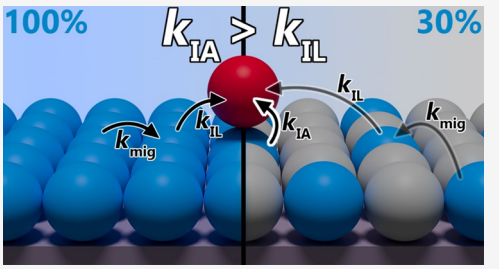

INTRODUCTION

Organic−inorganic interfaces are critical to a range of applications including biosensing, organic electronics, heterogeneous catalysis, and so on.[1,2] The binding of molecules to metal oxide interfaces through surface coordinating groups (e.g., −COOH, $-PO_3H_2$) is appealing because of their stability, strong interfacial coupling, and utility in applications like dye-sensitized solar and photochemical cells.[3−6] In many dye-sensitized schemes, it is advantageous to couple two or more molecular moieties, including a chromophore and catalyst, chromophore and electron donor/acceptor, or two complementary chromophores, to name a few. Example multimolecular interfacial assembly strategies include codeposition, electrostatic interactions, covalent dyads, and metal-ion-linked multilayers.[7] The latter is particularly appealing because of its ease of preparation (i.e., it avoids the synthetic complexity of covalent dyads), its modularity in component selection/design, and its layer-by-layer assembly method circumvents the surface area limitation of codeposition.[8−11] Furthermore, the layered nature enables directional energy and electron transfer toward or away from the substrate which are beneficial to their use in photocatalysis,[12−14] photon upconversion,[15−17] energy cascade solar cells,[18] rectifying interfaces,[19−22] electrochromism,[23] and electrochemiluminescence.[24]

As expected from the first-principles method, films reported to date indicate that the direction, rate, and efficiency of interfacial electron/energy transfer are dependent on both the energetics and the structure of the molecular units.[25−29] Consequently, to maximize the utility of these metal-ion-linked assemblies, one must be able to control the relative orientation of molecules in the multilayers. However, a critical first step toward structural design principles is differentiating between intra-assembly (IA; between metal-ion-linked molecules) and interlayer (IL; between separate layers of nonlinked molecules) energy/electron transfer events (Figure 1b). Here, we use time-resolved spectroscopy and a surface dilution strategy to differentiate between the IA and IL energy transfer. The idea is that dilution of a donor chromophore (A in Figure 1) with an inert spacer (S) will slow k_{IL} and possible cross-surface migration of excited states (k_{mig}) relative to k_{IA} enabling the use of surface loading concentration dependence to determine the dominant energy transfer mechanism in the bilayer film (ZrO_2-**A**-Zn-**P**).

METHODS

Materials. 4-Bromo-*p*-terphenyl (Synthonix, Inc.) and 1,3-diisopropyl benzene (Tokyo Chemical Industry) were purchased from their respective suppliers in parentheses and

Received: June 18, 2024
Revised: August 4, 2024
Accepted: August 9, 2024
Published: August 26, 2024

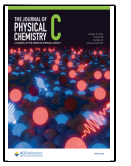

https://doi.org/10.1021/acs.jpcc.4c04033
J. Phys. Chem. C 2024, 128, 16861−16868

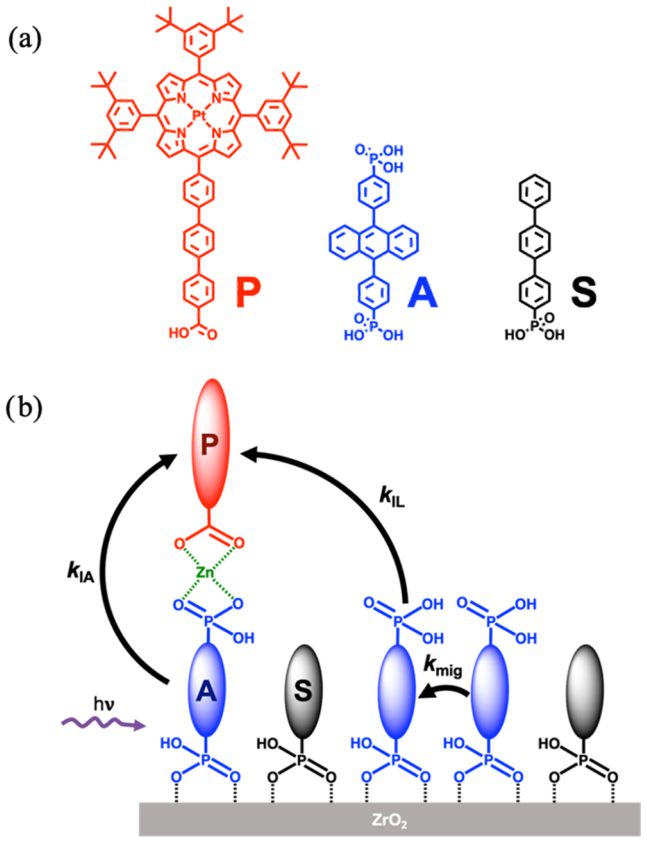

Figure 1. (a) Molecular structure of **P**, **A**, and **S**. (b) Schematic representation of the self-assembled bilayer depicting photoinduced intra-assembly (k_{IA}) and interlayer (k_{IL}) energy transfer as well as cross-surface excited-state migration (k_{mig}).

used without further purification. Pyrrole was purchased from Millipore Sigma and distilled prior to use. All other reagents and solvents were purchased from Millipore Sigma (analytical reagent grade) and used without further purification. Molecule **A** was synthesized following previously published procedures.[30] Molecules **S** and **P** were synthesized for the first time with modification from previously published procedures, as detailed in the Supporting Information.[31−35] Glass substrates were purchased from Hartford Glass Co. and cut to the size noted below. Meltonix film (1170−25) and Vac'n'Fill Syringe (65209) were purchased from Solaronix. ZrO_2 sol−gel paste and films were prepared following previously reported procedures as detailed in the Supporting Information.[18,36,37]

Bilayer Assembly. Bilayer films (ZrO_2-**A**-Zn-**P**) with maximum surface coverage of **A** (i.e., no dilution with **S**) were prepared by submerging the mesoporous ZrO_2 films in 5 mL of 300 μM **A** in DMSO for 24 h, 5 mL of a 400 μM solution of $Zn(CH_3COO)_2{\cdot}2H_2O$ in methanol for 2 h, and finally a 5 mL saturated solution of **P** in a $CHCl_3$:MeOH (1:1, v/v). After each soaking step, the films were rinsed with ethanol and dried under a stream of nitrogen. Surface diluted films of 60% and 30% were prepared using the same procedure except the first soaking step was replaced by a 5 mL solution containing variation in the volume ratio of 300 μM **A** in DMSO and 150 μM **S** in DMSO, as summarized in Table S1. Surface loading of **A** and the **A**:**P** ratios were determined using ultraviolet−visible (UV−vis) spectroscopy. Surface coverages of **A** (Γ in mol cm^{-2}) were estimated using $\Gamma = (A(\lambda)/\varepsilon(\lambda))/1000$, where ε is the molar extinction coefficient of **A** in DMSO at 375 nm (1.27×10^4 M^{-1} cm^{-1}) and $A(\lambda)$ is the absorbance of the film at 375 nm.[30,38] Surface coverages of **S** were estimated using the same expression where ε is the molar extinction coefficient of **S** in DMSO at 310 nm (0.973×10^4 M^{-1} cm^{-1}) and $A(\lambda)$ is the absorbance of the film at 310 nm. Additional details can be found in the Supporting Information.

Spectroscopic Cell Preparation. Sandwich cells for spectroscopic measurements were prepared in a nitrogen glovebox and filled with dry, air-free acetonitrile following previously published procedures.[16,30]

Spectroscopic Measurements. Instrumentation and measurement details for absorption, steady-state emission, time-resolved emission, and transient absorption are provided in the Supporting Information.

RESULTS AND DISCUSSION

Surface Loading. A schematic depiction of the bilayer used in this study is shown in Figure 1b. The multilayer assembly is composed of a phosphonated diphenylanthracene (**A**) first layer, a zinc(II) linking ion, and a carboxylated platinum(II) porphyrin (**P**) second molecular layer (Figure 1a). This anthracene-porphyrin pair was selected because (1) they are derivatives of our previously studied molecular photon upconversion bilayers,[7,16,25,30] (2) the energetics are appropriate for ^{1}**A*** → **P** Förster resonance energy transfer and ^{3}**P*** → **A** triplet energy transfer,[39] and (3) the carboxylate binding group of **P** will limit competitive desorption of the more strongly binding phosphonate group of **A**.[40] However, in contrast to the previously studied bilayer that contained Pt(II) tetrakis(4-carboxyphenyl)porphyrin, the nonsymmetric porphyrin used here has a single terphenyl carboxylate metal-ion-binding moiety. This design was chosen because having only one carboxyl binding group will limit the range of possible intramolecular orientations (i.e., no possibility of two −COOH groups binding). Furthermore, the terphenyl spacer between the porphyrin core and the carboxyl group will increase the spatial separation within the assembly, which is expected to slow interlayer energy transfer dynamics for ease of spectroscopic monitoring (vide infra). Terphenyl monophosphonic acid (**S**) was chosen as a photo- and electrochemically inert coadsorbent for surface dilution because it is similar in size and binding motif to **A**, it enables dilution of **A** while hindering direct surface adsorption of **P**, and it lacks the second phosphonate group necessary for Zn-**P** binding (i.e., it will not form a bilayer).

Bilayer films (ZrO_2-**A**-Zn-**P**) with maximum surface coverage of **A** (i.e., no dilution with **S**) were prepared by stepwise soaking of mesoporous ZrO_2 films in a DMSO solution of **A**, a MeOH solution of $Zn(CH_3COO)_2$, and finally a saturated solution of **P** in a $CHCl_3$/MeOH (1:1, v/v). The absorption spectra for ZrO_2-**A**, ZrO_2-**P**, and ZrO_2-**A**-Zn-**P** are shown in Figure 2. In line with previous loading studies, a maximum surface coverage of 1.1×10^{-7} mol cm^{-2} was achieved from a 300 μM DMSO solution of **A**.[39] In the absence of $Zn(CH_3COO)_2$ treatment, no absorption changes were observed when ZrO_2-**A** was soaked in a solution of **P** or fluorescein (300 μM in DMSO) indicating that coadsorption is hindered by complete monolayer coverage of **A** in these films. Consequently, this film loading condition was defined as 100% surface coverage of **A** and all dilutions (i.e., 60 and 30%) were defined relative to this maximum.[17]

https://doi.org/10.1021/acs.jpcc.4c04033
J. Phys. Chem. C 2024, 128, 16861−16868

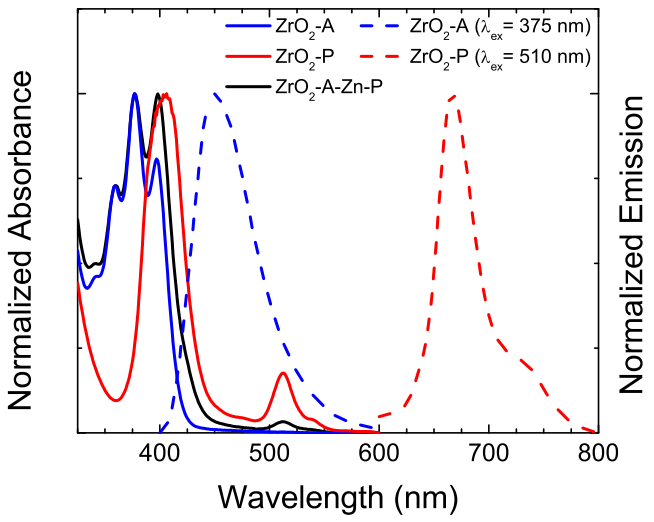

Figure 2. Absorption spectra (solid) of ZrO_2-**A**, ZrO_2-**P**, and ZrO_2-**A**-Zn-**P** and emission spectra (dashed) of ZrO_2-**A** and ZrO_2-**P** in MeCN.

Following the soaking of ZrO_2-**A** in $Zn(CH_3COO)_2$ and then **P** solutions, absorption features for **P** are observed in the UV−vis spectrum of the films which are consistent with ZrO_2-**A**-Zn-**P** bilayer formation (Figure 2). From spectral deconvolution, an **A**/**P** ratio of ∼14:1 was obtained. The relatively low loading of **P** was due in part to the low solubility of **P** in the loading solution but is also preferable to allow for the possibility of orientation changes of **P**, such as "laying down" relative to the surface for increased favorability for interlayer energy transfer (k_{IL} in Figure 1b).

ZrO_2-**A** films with surface dilutions of **A** were generated by soaking ZrO_2 in loading solutions containing various ratios of **A**:**S**, and the results are summarized in Figure 3. Based on the

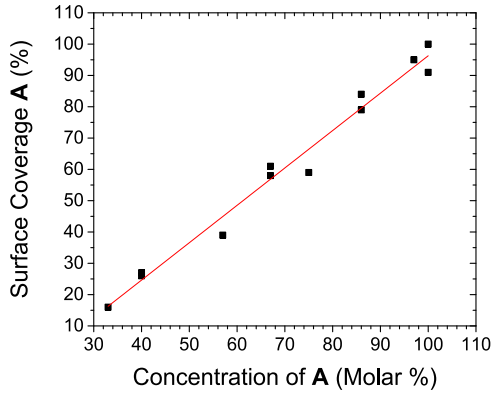

Figure 3. Percent surface coverage of **A** on ZrO_2 with respect to the mole % of **A** in the mixed **A**/**S** loading solution. The red line is a linear fit to the data (R^2 = 0.98, m = 1.2).

UV−vis absorption for **A**, there is a linear relationship between the percent surface coverage of **A** and the molar % **A** ([**A**] per ([**A**] + [**S**])) in the loading solution. Interestingly, the percent loading of **A** was consistently lower than the molar percent of the loading solution (slope = 1.2), suggesting that the binding affinity of **A** is less than that of **S**. This outcome is in agreement with the larger adsorption equilibrium constant for **S** (6.0×10^{-3}) than for **A** (2.6×10^{-3}) as determined from fitting the single component ZrO_2 loading isotherms (eq S1 and Figure S1).[27,30] This difference in K_{ad} is somewhat surprising given that **A** has two PO_3H_2 groups and **S** only has one, but it could be due to a slight difference in the size of the molecules. Regardless of the cause, the linear relationship between cosolution concentration and surface loading was used to consistently generate ZrO_2-**A** films with 100, 60, and 30% **A**-loaded films (see the UV−vis spectra in Figure S3) from 100, 67, and 42 molar % **A** loading solutions, herein denoted as ZrO_2-**A**(X%). It is important to note that upon excitation of ZrO_2-**A**(X%) with 360 nm light, the time-resolved emission decay from **A** was similar ($\tau_{avg} \approx 6$ ns) regardless of the surface loading (Figure S4 and Table S3). This observation indicates that dilution with **S** has a minimal impact on the photophysical properties of the surface-bound **A** molecules.

As observed above for the ZrO_2-**A**(100%), in the absence of $Zn(CH_3COO)_2$ treatment, soaking the 60 and 30% loaded films in a solution of **P** or fluorescein (300 μM in DMSO) resulted in no codeposition suggesting complete surface coverage of **A** and **S**. Following $Zn(CH_3COO)_2$ treatment, **P** readily loads on all surfaces and the total **P** loading ($\sim 1 \times 10^{-8}$ mol cm^{-2}) was kept consistent across all film dilutions.

Time-Resolved Spectroscopy. ^{1}**A*** to **P** energy transfer dynamics for the films in nitrogen-deaerated acetonitrile were first probed using time-resolved emission, and the results are shown in Figure 4. Upon 360 nm excitation, the ZrO_2-**A** film

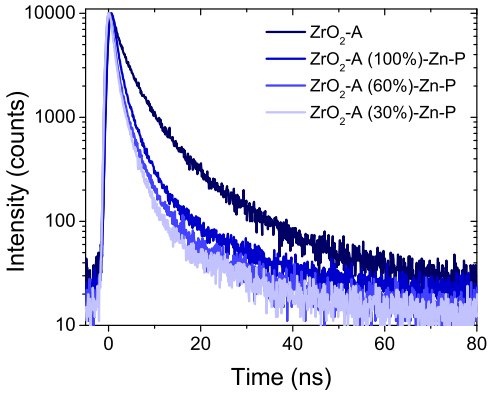

Figure 4. Time-resolved emission decay traces for ZrO_2-**A**(100%) and ZrO_2-**A**(X%)-Zn-**P** in MeCN at 460 nm (λ_{ex} = 360 nm).

exhibits emission features consistent with diphenylanthracene.[30] The decay kinetics at 460 nm could be fit with a biexponential function, with the amplitude (A_x) and lifetime (τ_x) for each component as well as the intensity weighted average lifetime ($\tau_{w(A)}$) summarized in Table 1. Even for a single emissive species, multiexponential kinetics are common for surface-bound molecules and often attributed to inhomogeneous local environments in the film.[39,41]

In the bilayer film (i.e., ZrO_2-**A**(100%)-Zn-**P**), the average lifetime for **A** emission decreases to 3.9 ns relative to ZrO_2-**A** ($\tau_{w(A)}$ = 5.7 ns). This observation is consistent with our, and others', previous reports where Pt(II) porphyrin serves as a FRET acceptor from **A***.[30,39,42] With surface dilution of **A**, there is a decrease in τ_1 and τ_2 as well as an increase in the amplitude of the fast component (A_1) resulting in a decreased average lifetime in the order of 100% > 60% > 30% **A** loading. These results suggest that as the surface is diluted, there is faster and/or more efficient **A*** to **P** energy transfer. Assuming that **A** to **P** energy transfer is the only newly introduced

https://doi.org/10.1021/acs.jpcc.4c04033
J. Phys. Chem. C 2024, 128, 16861−16868

Table 1. Fitting Parameters for the Emission Decay at 460 nm for ZrO_2-A(100%) and ZrO_2-A(*X*%)-Zn-P in MeCN (λ_{ex} = 360 nm)[a]

sample	$\tau_{w(A)}$ (ns)[b]	A_1	τ_1 (ns)	A_2	τ_2 (ns)
ZrO_2-**A**	5.72 ± 2.11	0.55	1.40 ± 0.45	0.45	6.76 ± 2.1
ZrO_2-**A** (100%)−Zn-**P**	3.97 ± 0.28	0.67	0.97 ± 0.15	0.33	5.15 ± 0.5
ZrO_2-**A** (60%)−Zn-**P**	3.50 ± 0.14	0.68	0.88 ± 0.01	0.32	4.57 ± 0.1
ZrO_2-**A** (30%)−Zn-**P**	2.96 ± 0.08	0.70	0.81 ± 0.08	0.30	3.97 ± 0.1

[a]All results are the average of three independent sample preparations and measurements with the error bars being the standard deviation. Reported A_x and τ_x values are the average from three independent samples/fits. [b]$\tau_{w(A)}$ is the average of the intensity average lifetime of three independent samples and was calculated using $\langle\tau_w\rangle = \sum A_i\tau_i^2/\sum A_i\tau_i$.

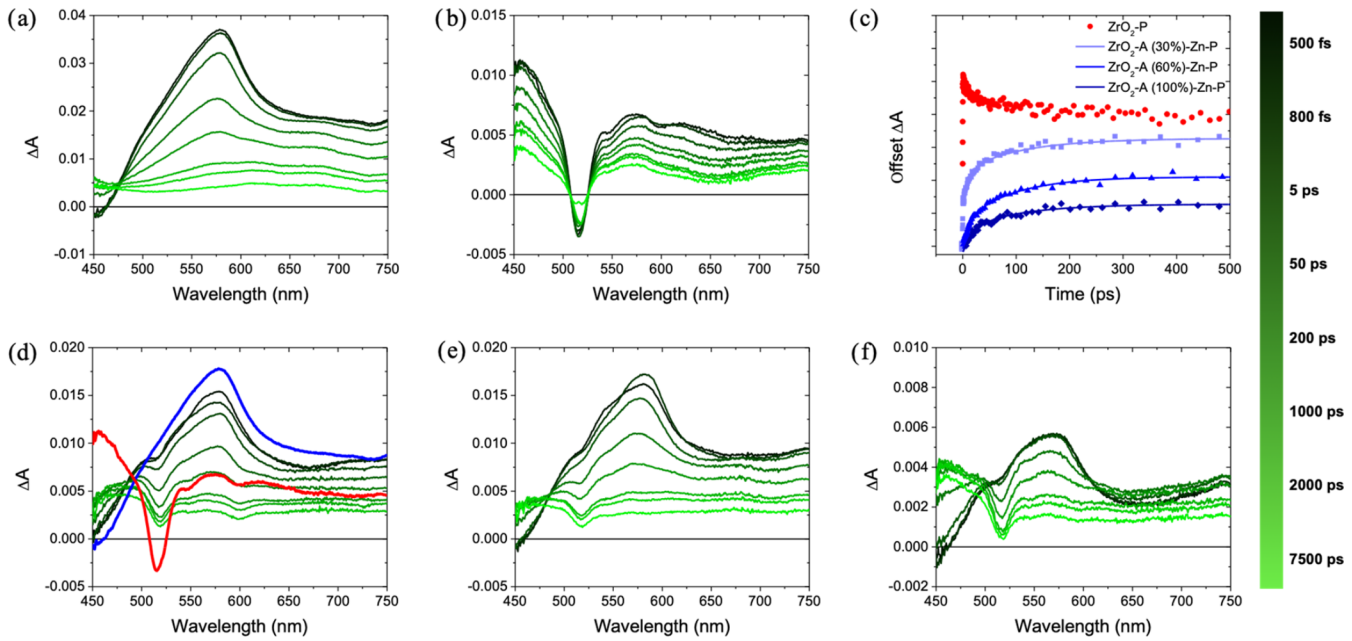

Figure 5. (a, b) Transient absorption spectra for (a) ZrO_2-**A** (λ_{ex} = 360 nm) and (b) ZrO_2-**P** (λ_{ex} = 512 nm). (c) ΔA at 460 nm for ZrO_2-**A**(*X* %)-Zn-**P** with respect to time following 360 nm excitation with the biexponential fits in solid lines. Also included is the ΔA at 577 nm for ZrO_2-**P** under 405 nm excitation (ΔA values are offset on the *y*-axis for visual clarity). Transient absorption spectra for ZrO_2-**A**(*X*%)-Zn-**P** in MeCN, where (d) *X* = 30%, (e) *X* = 60%, and (f) *X* = 100% (λ_{ex} = 360 nm). Blue and red overlays in (d) are spectra at 500 fs for ZrO_2-**A** and ZrO_2-**P**, respectively. The spectral time slices were kept consistent across all samples, with the time-color legend depicted on the right. All samples were measured in nitrogen-deaerated MeCN.

quenching mechanism in the bilayer film, the rate constant for energy transfer (k_{ET}) can be estimated using eq 1

$$k_{ET} = \frac{1}{\tau_{bl}} - \frac{1}{\tau_A} \quad (1)$$

where τ_A and τ_{bl} are the average lifetimes for anthracene emission in the ZrO_2-**A** and ZrO_2-**A**(*X*%)-Zn-**P** films, respectively.[39] The calculated energy transfer rate increases in the order 100% (0.7×10^8 s^{-1}) < 60% (1.1×10^8 s^{-1}) < 30% (1.5×10^8 s^{-1}) **A** loading. However, this calculation assumes that all A* atoms are directly involved in the energy transfer process. Given that not every **A** is in proximity with **P**, there is likely a subpopulation of **A*** which decays independently and/or must undergo cross-surface energy migration (k_{mig} in Figure 1b) before **A*** to **P** energy transfer, both of which would result in a lengthening of the observed A* lifetime in the bilayer. Consequently, the energy transfer rates listed above are likely low-end estimates of k_{ET}.

To further probe the **A*** to **P** energy transfer dynamics, we performed transient absorption spectroscopy, and the results are shown in Figure 5. For the **A**-only film (ZrO_2-**A**) excited at 360 nm, there are ground-state bleach and excited-state absorption features below and above 460 nm, respectively (Figure 5a). All features decay with an average lifetime of ∼5 ns, which is consistent with fluorescent emission from ^{1}**A*** observed by time-resolved emission (vide supra). Upon 515 nm excitation, the ZrO_2-**P** film exhibits a ground-state bleach at 515 nm (i.e., the Q-band) and a broad excited-state absorption from 450 to 800 nm (Figure 5b). These features are retained beyond the 7 ns window of the instrument response which is consistent with the formation of a long-lived, triplet excited state of the porphyrin (^{3}**P***; $\tau \approx 40$ μs).[30] The consistency of the spectral features of ZrO_2-**P** suggests that excitation to the singlet excited state followed by rapid intersystem crossing to ^{3}**P*** occurs within the instrument response function (∼250 fs) followed by decay from the ^{3}**P*** state, which is in line with the previously reported Pt(II) porphyrin excited-state dynamics.[43]

For all three ZrO_2-**A**(*X*%)-Zn-**P** films under 360 nm irradiation (i.e., preferential excitation of **A**), early time slices resemble the spectral features of ^{1}**A*** which evolve over time to that of ^{3}**P*** (Figure 5d−f). Relative to the ZrO_2-**A** film (τ = 6 ns), the excited-state absorption feature of **A** at 575 nm in the ZrO_2-**A**(*X*%)-Zn-**P** films more rapidly decays (τ < 500 ps),

https://doi.org/10.1021/acs.jpcc.4c04033
J. Phys. Chem. C 2024, 128, 16861−16868

which is consistent with ^{1}**A*** to **P** energy transfer. The isosbestic point of ZrO_2-**A** at 460 nm was used to preferentially monitor the growth of the ESA of **P**, and the results are shown in Figure 5c. In contrast to the instrument-limited appearance of ^{3}**P*** via direct excitation of ZrO_2-**P** (red trace in Figure 5c), the ZrO_2-**A**(*X*%)-Zn-**P** films exhibit a relatively slow rise of ^{3}**P***, which largely plateaus by 400 ps in all three bilayers and whose features are still observed on the nano to microsecond time scales (Figure S5). The delayed growth supports a sensitized excitation mechanism, namely, excitation of **A**, ^{1}**A*** to **P** energy transfer, rapid intersystem crossing from ^{1}**P*** to ^{3}**P***, followed by slow excited-state decay from ^{3}**P***.

The rise in ΔA at 460 nm (Figure 5c) could be fit with a biexponential function, and the results are summarized in Table 2. Notably, there is no obvious trend in the kinetics with

Table 2. Fitting Parameters for Transient Absorption Kinetics at 460 nm for ZrO_2-A(*X*%)-Zn-P (λ_{ex} = 360 nm)[a]

X (%)	τ_w (ps)[b]	A_1	τ_1 (ps)	A_2	τ_2
100	148.9 ± 55.1	0.11	17.2 ± 10.5	0.89	151.4 ± 55.3
60	105.1 ± 9.4	0.14	19.4 ± 5.6	0.86	107.9 ± 10.7
30	112.9 ± 5.2	0.11	15.1 ± 2.8	0.89	114.6 ± 4.4

[a]All results are the average of three independent sample preparations and measurements with the error bars being the standard deviation. Reported A_x and τ_x values are the average from three independent samples/fits. [b]$\tau_{w(A)}$ is the average of the intensity average lifetime of three independent samples and was calculated using $\langle\tau_w\rangle = \sum A_i\tau_i^2/\sum A_i\tau_i$.

respect to surface dilution, other than the amplitude in the error increasing with *A* loading (i.e., increased sample-to-sample variability). In fact, for τ_1, τ_2, and τ_w, all values are similar within the error of the samples/measurement. This observation suggests that surface dilution had little to no impact on the ^{1}**A*** to **P** energy transfer rate, at least on the sub-nanosecond time scale.

The energetics for the ZrO_2-**A**(*X*%)-Zn-**P** are also favorable such that ^{3}**P*** → **A** triplet energy transfer (TET) can serve as a secondary probe of interlayer vs intra-assembly energy transfer.[39] Following excitation of **P** at 512 nm (i.e., into the Q-band), emission decay kinetics were monitored at 670 nm from ZrO_2-**P** and ZrO_2-**A**(*X*%)-Zn-**P**, and the results are shown in Figure 6. In the bilayer film, the weighted average emission lifetime for **P** ($\tau_{w(P)}$) decreases from 44 μs to ~34 μs for the ZrO_2-**P** film (Table S4), which is consistent with

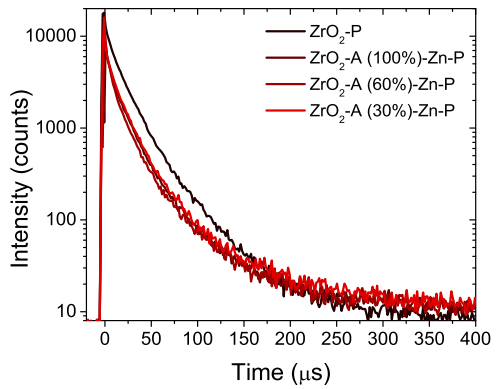

Figure 6. Time-resolved emission decay traces for ZrO_2-**P** and ZrO_2-**A**(*X*%)-Zn-**P** at 670 nm in nitrogen-deaerated MeCN (λ_{ex} = 512 nm).

excited-state quenching via ^{3}**P*** → **A** TET. Interestingly, the excited-state lifetimes were similar regardless of the surface dilution. Using eq 1, the estimated energy transfer rate is ~6×10^3 s^{-1}, resulting in a calculated TET quantum yield of ~0.2 (see Table S4 for details). The relatively consistent ^{3}**P*** → **A** TET rate/yield at all surface dilutions suggests that the concentration of nonlinked anthracene molecules has minimal impact on the TET event.

Energy Transfer Discussion. The hypothetical impact of surface dilution on the ^{1}**A*** to **P** energy transfer dynamics in the bilayer film is depicted in Figure 7. For the fully loaded

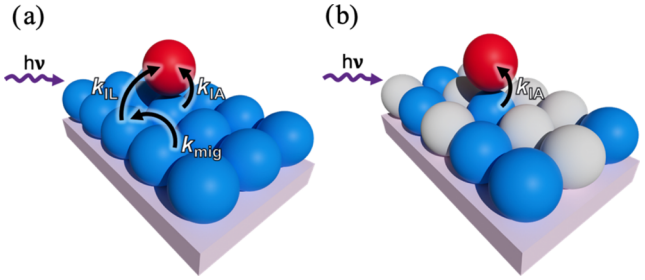

Figure 7. Illustrations of (a) ZrO_2-**A**(100%)-Zn-**P** and (b) ZrO_2-**A**(30%)-Zn-**P** highlighting possible intra-assembly (k_{IA}) and interlayer (k_{IL}) energy transfer as well as cross-surface excited-state migration (k_{mig}) following excitation of **A**.

anthracene film, one can envision either k_{IA} or k_{IL} being the more rapid ^{1}**A*** to **P** energy transfer process. Concurrently, because the **P**-to-**A** ratio is 1:14, not all **A** are in proximity with a **P** molecule and thus some portion of ^{1}**A*** can undergo its intrinsic decay processes (k_r or k_{nr}). Alternatively, through cross-surface energy transfer, ^{1}**A*** could migrate toward a **P** molecule (k_{mig}) followed by intra-assembly or interlayer energy transfer.

Surface dilution with **S** is expected to have minimal impact on k_{IA} because the distance and relative orientation between molecules in the metal-ion-linked assembly are expected to be unperturbed. However, surface dilution of **A** from 100 to 30% will decrease the average number of nonlinked **P**-adjacent-**A** molecules from 8 to 2. Thus, the probability of favorable distance for interlayer energy transfer will decrease, slowing the average rate constant (k_{IL}) with **A** dilution. Likewise, cross-surface migration (k_{mig}) is dependent on the surface coverage of **A**, with k_{mig} decreasing with surface dilution until it is completely hindered below its percolation threshold. For previously reported monolayer films, the percolation threshold for cross-surface electron and triplet energy transfer are generally >60%.[7] However, those electron transfer and exchange mechanisms exhibit higher sensitivity to intermolecular separation than a singlet exchange mechanism expected for ^{1}**A***. Additionally the short lifetime of ^{1}**A*** will decrease the number of random hops and distance traveled relative to a triplet or cationic state. Regardless of uncertainties in the magnitude of the change, one would expect a decrease in k_{mig} with dilution.

From the time-resolved emission measurements of **A** in ZrO_2-**A**(*X*%)-Zn-**P**, we observe a decrease in the emission lifetime of ^{1}**A*** with respect to surface loading. That observation is consistent with the increased quenching of **A** with surface loading and k_{IL} and k_{mig} being pivotal energy transfer pathway. However, the emission measurements capture the average behavior of ^{1}**A***, including those not

https://doi.org/10.1021/acs.jpcc.4c04033
J. Phys. Chem. C 2024, 128, 16861−16868

involved in the transfer of energy to **P**. Consequently, the decreased lifetime could be attributed to fast k_{IA} and slow or completely inhibited k_{mig}/k_{IL}, which results in nonlinked ^{1}**A*** undergoing intrinsic emissive decay. In that scenario, quenching via k_{IA} would remain constant (i.e., a short lifetime for bound ^{1}**A***), but the portion of **A** molecules undergoing intrinsic decay would decrease with surface dilution resulting in a decrease in $\tau_{w(A)}$ with dilution, as observed here.

With transient absorption measurements, we observed that the growth of porphyrin excited-state features (i.e., excitation via energy transfer) was similar regardless of the surface dilution of **A**. In line with the discussion presented above, it is difficult to envision a scenario where k_{IL} and k_{mig} are unperturbed by surface dilution. Consequently, the TA data indicate that direct k_{IA} is faster than k_{IL} and the intra-assembly mechanism is the dominant contributor to ^{1}**A*** to **P** energy transfer on sub-nanosecond time scales. Interestingly, the dilution-independent appearance of ^{3}**P*** could also be observed if $k_{mig} \gg k_{IA}$ (i.e., rapid energy migration from unlinked to linked **A**, followed by rate limiting k_{IA}). However, given the dramatically lower favorability for **A** to **A** versus **A** to **P** energy transfer (i.e., lower spectral overlap), we find that scenario unlikely. Therefore, we suggest that k_{IA} is more rapid than k_{mig} and k_{IL}. It is however worth noting that k_{mig} and k_{IL} can likely occur, but would do so on a longer time scale than k_{IA}.

Rapid intra-assembly energy transfer is further observed in the ^{3}**P*** to **A** TET rate/yield measurement. Because TET is dependent on the distance and electronic coupling between the donor (**P**) and acceptor (**A**), diluting the surface (i.e., increasing distance and decreasing coupling) is expected to decrease the interlayer TET rate.[44] Experimentally, the TET was found to be independent of surface dilution, suggesting that TET within the **A**-Zn-**P** assembly is the more rapid and dominant energy transfer mechanism due to a shorter distance and/or better electronic coupling than with adjacent **A** molecules.

CONCLUSIONS

Here, we used systematic surface dilution with a spectroscopic inert spacer molecule (**S**) to probe intra-assembly (IA) and interlayer (IL) energy transfer events in a ZrO_2-**A**-Zn-**P** metal-ion-linked bilayer. Surface dilution was achieved by controlling the concentrations of **A** and **S** in the loading solution. Interestingly, as measured by both time-resolved emission and transient absorption, surface dilution had minimal impact on the rate of ^{1}**A*** to **P** and ^{3}**P*** to **A**, singlet, and triplet energy transfer rates, respectively. Because some **A** and **P** molecules are geometrically linked, surface dilution with **S** is expected to have a minimal impact on k_{IA}. Conversely, surface dilution of **A** with **S** will increase the distance between nonlinked **A** and **P** as well as **A** and **A**, slowing k_{IL} and cross-surface migration (k_{mig}). Therefore, the relatively constant energy transfer rates, regardless of dilution, indicate that intra-assembly FRET and TET are the faster and dominant energy transfer processes in metal-ion-linked multilayers. Unfortunately, we cannot definitively conclude that intra-assembly is the dominant energy transfer mechanism in all metal-ion-linked multilayers. However, the samples reported here were intentionally selected/designed to bias toward interlayer energy transfer (i.e., long molecules that could lay down and perpendicular transition moments more favorable for FRET). The lack of interlayer energy transfer in these films leads us to believe that intra-assembly energy transfer will be the dominant mechanism in most, if not all, metal-ion-linked multilayers. We can envision this outcome as being important for two reasons. First, because energy transfer is primarily occurring within the assembly, the transition dipole moment orientation dependence of FRET can be used to gain structural insights into the relative orientation of molecules in the metal-ion-linked assembly. Second, future design strategies can be guided by the knowledge that it is primarily the orientation of the linked molecules that dictates the rate and efficiency of interlayer energy transfer.

ASSOCIATED CONTENT

Supporting Information

The Supporting Information is available free of charge at https://pubs.acs.org/doi/10.1021/acs.jpcc.4c04033.

Synthetic and spectroscopic measurement details; sample preparation procedure; adsorption isotherms; and additional kinetic decays/fitting and spectra (PDF)

AUTHOR INFORMATION

Corresponding Author

Kenneth Hanson − *Department of Chemistry & Biochemistry, Florida State University, Tallahassee, Florida 32306-4390, United States;* orcid.org/0000-0001-7219-7808; Email: hanson@chem.fsu.edu

Authors

Grace M. McLeod − *Department of Chemistry & Biochemistry, Florida State University, Tallahassee, Florida 32306-4390, United States;* orcid.org/0000-0003-4018-8864

Jackson Nolder − *Department of Chemistry & Biochemistry, Florida State University, Tallahassee, Florida 32306-4390, United States*

Ashley Arcidiacono − *Department of Chemistry & Biochemistry, Florida State University, Tallahassee, Florida 32306-4390, United States;* orcid.org/0000-0001-8617-2097

Sarah Lindbom − *Department of Chemistry & Biochemistry, Florida State University, Tallahassee, Florida 32306-4390, United States*

Nikolas R. Dos Santos − *Department of Chemistry & Biochemistry, Florida State University, Tallahassee, Florida 32306-4390, United States*

Ethan C. Lambert − *Department of Chemistry & Biochemistry, Florida State University, Tallahassee, Florida 32306-4390, United States;* orcid.org/0000-0001-6893-9071

Suliman Ayad − *Department of Chemistry & Biochemistry, Florida State University, Tallahassee, Florida 32306-4390, United States*

Drake Beery − *Department of Chemistry & Biochemistry, Florida State University, Tallahassee, Florida 32306-4390, United States*

Igor V. Alabugin − *Department of Chemistry & Biochemistry, Florida State University, Tallahassee, Florida 32306-4390, United States;* orcid.org/0000-0001-9289-3819

Complete contact information is available at: https://pubs.acs.org/10.1021/acs.jpcc.4c04033

Notes

The authors declare no competing financial interest.

https://doi.org/10.1021/acs.jpcc.4c04033
J. Phys. Chem. C 2024, 128, 16861−16868

■ ACKNOWLEDGMENTS

Energy transfer measurements were supported by the National Science Foundation under grant no. DMR-2327754. Characterization of the bilayer formation was supported by the Army Research Office under grant no. W911NF-19-1-0357. A.I. is grateful to the National Science Foundation (CHE-2102579) for the support of fundamental research.

■ REFERENCES

(1) Niederhausen, J.; Mazzio, K. A.; MacQueen, R. W. Inorganic−Organic Interfaces in Hybrid Solar Cells. *Electron. Struct.* **2021**, *3* (3), No. 033002.
(2) Huang, Z.; Miyashita, T.; Tang, M. L. Photon Upconversion at Organic-Inorganic Interfaces. *Annu. Rev. Phys. Chem.* **2024**, *75* (1), 329−346.
(3) Bobo, M. V.; Paul, A.; Robb, A. J.; Arcidiacono, A. M.; Smith, M. D.; Hanson, K.; Vannucci, A. K. Bis-Cyclometalated Iridium Complexes Containing 4,4′-Bis(Phosphonomethyl)-2,2′-Bipyridine Ligands: Photophysics, Electrochemistry, and High-Voltage Dye-Sensitized Solar Cells. *Inorg. Chem.* **2020**, *59* (9), 6351−6358.
(4) Ashford, D. L.; Gish, M. K.; Vannucci, A. K.; Brennaman, M. K.; Templeton, J. L.; Papanikolas, J. M.; Meyer, T. J. Molecular Chromophore−Catalyst Assemblies for Solar Fuel Applications. *Chem. Rev.* **2015**, *115* (23), 13006−13049.
(5) Beery, D.; Wheeler, J. P.; Arcidiacono, A.; Hanson, K. CdSe Quantum Dot Sensitized Molecular Photon Upconversion Solar Cells. *ACS Appl. Energy Mater.* **2020**, *3* (1), 29−37.
(6) Ogunsolu, O. O.; Wang, J. C.; Hanson, K. Increasing the Open-Circuit Voltage of Dye-Sensitized Solar Cells via Metal-Ion Coordination. *Inorg. Chem.* **2017**, *56* (18), 11168−11175.
(7) Wang, J. C.; Hill, S. P.; Dilbeck, T.; Ogunsolu, O. O.; Banerjee, T.; Hanson, K. Multimolecular Assemblies on High Surface Area Metal Oxides and Their Role in Interfacial Energy and Electron Transfer. *Chem. Soc. Rev.* **2018**, *47* (1), 104−148.
(8) Lee, H.; Kepley, L. J.; Hong, H. G.; Mallouk, T. E. Inorganic Analogs of Langmuir-Blodgett Films: Adsorption of Ordered Zirconium 1,10-Decanebisphosphonate Multilayers on Silicon Surfaces. *J. Am. Chem. Soc.* **1988**, *110* (2), 618−620.
(9) Hanson, K.; Torelli, D. A.; Vannucci, A. K.; Brennaman, M. K.; Luo, H.; Alibabaei, L.; Song, W.; Ashford, D. L.; Norris, M. R.; Glasson, C. R. K.; Concepcion, J. J.; Meyer, T. J. Self-Assembled Bilayer Films of Ruthenium(II)/Polypyridyl Complexes through Layer-by-Layer Deposition on Nanostructured Metal Oxides. *Angew. Chem. Int. Ed* **2012**, *51* (51), 12782−12785.
(10) Robb, A. J.; Knorr, E. S.; Watson, N.; Hanson, K. Metal Ion Linked Multilayers on Mesoporous Substrates: Energy/Electron Transfer, Photon Upconversion, and More. *J. Photochem. Photobiol., A* **2020**, *390*, No. 112291.
(11) Arcidiacono, A.; Hanks, B.; Hanson, K. Metal Ion-Linked Molecular Multilayers on Inorganic Substrates: Structure and Applications. *ACS Appl. Opt. Mater.* **2023**, *1* (6), 1156−1168.
(12) Ding, X.; Gao, Y.; Zhang, L.; Yu, Z.; Liu, J.; Sun, L. Visible Light-Driven Water Splitting in Photoelectrochemical Cells with Supramolecular Catalysts on Photoanodes. *ACS Catal.* **2014**, *4* (7), 2347−2350.
(13) Yoshimura, N.; Yoshida, M.; Kato, M.; Kobayashi, A. Photocatalyst−Mediator Interface Modification by Surface-Metal Cations of a Dye-Sensitized H_2 Evolution Photocatalyst. *Inorg. Chem.* **2022**, *61* (29), 11095−11102.
(14) Gross, M. A.; Creissen, C. E.; Orchard, K. L.; Reisner, E. Photoelectrochemical Hydrogen Production in Water Using a Layer-by-Layer Assembly of a Ru Dye and Ni Catalyst on NiO. *Chem. Sci.* **2016**, *7* (8), 5537−5546.
(15) Beery, D.; Schmidt, T. W.; Hanson, K. Harnessing Sunlight via Molecular Photon Upconversion. *ACS Appl. Mater. Interfaces* **2021**, *13* (28), 32601−32605.
(16) Hill, S. P.; Dilbeck, T.; Baduell, E.; Hanson, K. Integrated Photon Upconversion Solar Cell via Molecular Self-Assembled Bilayers. *ACS Energy Lett.* **2016**, *1* (1), 3−8.
(17) Zhou, Y.; Ruchlin, C.; Robb, A. J.; Hanson, K. Singlet Sensitization-Enhanced Upconversion Solar Cells via Self-Assembled Trilayers. *ACS Energy Lett.* **2019**, *4* (6), 1458−1463.
(18) Ogunsolu, O. O.; Murphy, I. A.; Wang, J. C.; Das, A.; Hanson, K. Energy and Electron Transfer Cascade in Self-Assembled Bilayer Dye-Sensitized Solar Cells. *ACS Appl. Mater. Interfaces* **2016**, *8* (42), 28633−28640.
(19) Ogunsolu, O. O.; Wang, J. C.; Hanson, K. Inhibiting Interfacial Recombination Events in Dye-Sensitized Solar Cells Using Self-Assembled Bilayers. *ACS Appl. Mater. Interfaces* **2015**, *7* (50), 27730−27734.
(20) Wang, J. C.; Murphy, I. A.; Hanson, K. Modulating Electron Transfer Dynamics at Dye−Semiconductor Interfaces via Self-Assembled Bilayers. *J. Phys. Chem. C* **2015**, *119* (7), 3502−3508.
(21) Farnum, B. H.; Wee, K.-R.; Meyer, T. J. Self-Assembled Molecular p/n Junctions for Applications in Dye-Sensitized Solar Energy Conversion. *Nat. Chem.* **2016**, *8* (9), 845−852.
(22) Sampaio, R. N.; Troian-Gautier, L.; Meyer, G. J. A Charge-Separated State That Lives for Almost a Second at a Conductive Metal Oxide Interface. *Angew. Chem. Int. Ed* **2018**, *57* (47), 15390−15394.
(23) Li, Z.-J.; Yao, C.-J.; Zhong, Y.-W. Near-Infrared Electrochromism of Multilayer Films of a Cyclometalated Diruthenium Complex Prepared by Layer-by-Layer Deposition on Metal Oxide Substrates. *Sci. China Chem.* **2019**, *62* (12), 1675−1685.
(24) Ning, H.; Liu, F.; Zhang, T.; Zhao, Y.; Li, Y.; Zhao, Z.; Liu, C.; Zhang, W.; Wang, H.; Li, F. A Signal-Amplification Electrochemiluminescence Sensor Based on Layer-by-Layer Assembly of Perylene Diimide Derivatives for Dopamine Detection at Low Potential. *Anal. Chim. Acta* **2022**, *1214*, No. 339963.
(25) Arcidiacono, A.; Zhou, Y.; Zhang, W.; Ellison, J. O.; Ayad, S.; Knorr, E. S.; Peters, A. N.; Zheng, L.; Yang, W.; Saavedra, S. S.; Hanson, K. Examining the Influence of Bilayer Structure on Energy Transfer and Molecular Photon Upconversion in Metal Ion Linked Multilayers. *J. Phys. Chem. C* **2020**, *124* (43), 23597−23610.
(26) Pattadar, D.; Arcidiacono, A.; Beery, D.; Hanson, K.; Saavedra, S. S. Molecular Orientation and Energy Transfer Dynamics of a Metal Oxide Bound Self-Assembled Trilayer. *Langmuir* **2023**, *39* (30), 10670−10679.
(27) Zhou, Y.; Ayad, S.; Ruchlin, C.; Posey, V.; Hill, S. P.; Wu, Q.; Hanson, K. Examining the Role of Acceptor Molecule Structure in Self-Assembled Bilayers: Surface Loading, Stability, Energy Transfer, and Upconverted Emission. *Phys. Chem. Chem. Phys.* **2018**, *20* (31), 20513−20524.
(28) Pattadar, D.; Zheng, L.; Robb, A. J.; Beery, D.; Yang, W.; Hanson, K.; Saavedra, S. S. Molecular Orientation of $-PO_3H_2$ and $-COOH$ Functionalized Dyes on TiO_2, Al_2O_3, ZrO_2, and ITO: A Comparative Study. *J. Phys. Chem. C* **2023**, *127* (5), 2705−2715.
(29) Arcidiacono, A.; Robb, A. J.; Masitas, R. A.; Salpage, S. R.; McLeod, G. M.; Chen, J.; Ogunsolu, O. O.; Roper, M. G.; Hanson, K. Inhibited Interlayer Electron Transfer in Metal Ion Linked Multilayers on Mesoporous Metal Oxide Films. *J. Photochem. Photobiol.* **2022**, *9*, No. 100088.
(30) Hill, S. P.; Banerjee, T.; Dilbeck, T.; Hanson, K. Photon Upconversion and Photocurrent Generation via Self-Assembly at Organic−Inorganic Interfaces. *J. Phys. Chem. Lett.* **2015**, *6* (22), 4510−4517.
(31) Wang, Z.; Heising, J. M.; Clearfield, A. Sulfonated Microporous Organic−Inorganic Hybrids as Strong Bronsted Acids [1]. *J. Am. Chem. Soc.* **2003**, *125* (34), 10375−10383.
(32) Vela, S.; Bauroth, S.; Atienza, C.; Molina-Ontoria, A.; Guldi, D. M.; Martín, N. Determining the Attenuation Factor in Molecular Wires Featuring Covalent and Noncovalent Tectons. *Angew. Chem. Int. Ed* **2016**, *55* (48), 15076−15080.

https://doi.org/10.1021/acs.jpcc.4c04033
J. Phys. Chem. C 2024, 128, 16861−16868

(33) Zhang, Q.; Wu, F.-Y.; Liu, J.-C.; Li, R.-Z.; Jin, N.-Z. Two Novel Self-Assemblies of Supramolecular Solar Cells Using N-Heterocyclic-Anchoring Porphyrins. *Spectrochim. Acta, Part A* **2018**, *191*, 398−404.
(34) Lindsey, J. S. Synthetic Routes to *Meso* -Patterned Porphyrins. *Acc. Chem. Res.* **2010**, *43* (2), 300−311.
(35) Rothemund, P. A New Porphyrin Synthesis. The Synthesis of Porphin[1]. *J. Am. Chem. Soc.* **1936**, *58* (4), 625−627.
(36) Song, W.; Glasson, C. R. K.; Luo, H.; Hanson, K.; Brennaman, M. K.; Concepcion, J. J.; Meyer, T. J. Photoinduced Stepwise Oxidative Activation of a Chromophore−Catalyst Assembly on TiO_2. *J. Phys. Chem. Lett.* **2011**, *2* (14), 1808−1813.
(37) Heimer, T. A.; D'Arcangelis, S. T.; Farzad, F.; Stipkala, J. M.; Meyer, G. J. An Acetylacetonate-Based Semiconductor−Sensitizer Linkage. *Inorg. Chem.* **1996**, *35* (18), 5319−5324.
(38) Gallagher, L. A.; Serron, S. A.; Wen, X.; Hornstein, B. J.; Dattelbaum, D. M.; Schoonover, J. R.; Meyer, T. J. Photoelectrochemistry on Ru^{II} −2,2′-Bipyridine-Phosphonate-Derivatized TiO_2 with the I_3^-/I^- and Quinone/Hydroquinone Relays. Design of Photoelectrochemical Synthesis Cells. *Inorg. Chem.* **2005**, *44* (6), 2089−2097.
(39) Dilbeck, T.; Wang, J. C.; Zhou, Y.; Olsson, A.; Sykora, M.; Hanson, K. Elucidating the Energy- and Electron-Transfer Dynamics of Photon Upconversion in Self-Assembled Bilayers. *J. Phys. Chem. C* **2017**, *121* (36), 19690−19698.
(40) Hanson, K.; Brennaman, M. K.; Luo, H.; Glasson, C. R. K.; Concepcion, J. J.; Song, W.; Meyer, T. J. Photostability of Phosphonate-Derivatized, Ru^{II} Polypyridyl Complexes on Metal Oxide Surfaces. *ACS Appl. Mater. Interfaces* **2012**, *4* (3), 1462−1469.
(41) Durrant, J. R.; Haque, S. A.; Palomares, E. Towards Optimisation of Electron Transfer Processes in Dye Sensitised Solar Cells. *Coord. Chem. Rev.* **2004**, *248* (13), 1247−1257.
(42) Dilbeck, T.; Hill, S. P.; Hanson, K. Harnessing Molecular Photon Upconversion at Sub-Solar Irradiance Using Dual Sensitized Self-Assembled Trilayers. *J. Mater. Chem. A* **2017**, *5* (23), 11652−11660.
(43) Singh-Rachford, T. N.; Castellano, F. N. Photon Upconversion Based on Sensitized Triplet−Triplet Annihilation. *Coord. Chem. Rev.* **2010**, *254* (21−22), 2560−2573.
(44) Dexter, D. L. A Theory of Sensitized Luminescence in Solids. *J. Chem. Phys.* **1953**, *21* (5), 836−850.

https://doi.org/10.1021/acs.jpcc.4c04033
J. Phys. Chem. C 2024, 128, 16861−16868